Visible Light Imaging

T. A. ten Brummelaar
CHARA, Georgia State University, Atlanta, GA 30303

K.1. INTRODUCTION

The function of the visible light imaging subsystem is to measure visibility magnitudes for all 21 baselines of the CHARA Array. In order to have the most complete imaging data set possible it would be advantageous to also measure fringe phase. Unfortunately, due to the random phase shifts introduced by the atmosphere, individual phases will be overwhelmed by noise, and the phase closure technique developed for radio interferometry (Thomson et al. 1986) will need to be employed. The modes of operation planned for the imaging subsystem are:

1. Visibility Magnitude and Phase Closure With Long Samples

   When enough light is available for the fringe tracker to lock onto the fringes the imaging subsystem can integrate over sample times that are long compared with the fringe tracking sample time and establish phase closure and visibility magnitudes for all baselines. If the fringe tracker loses phase lock, the integration can be stopped until the fringes are once again stable.

2. Visibility Magnitude and Phase Closure With Short Samples

   When too little light is available to lock onto the fringes, it should still be possible to track within a small part of the fringe envelope. The fringe phase will be changing at the time scale of the atmospheric turbulence t_0. If each sample was of this time scale or less, the magnitudes and closure phases can be measured by integrating over many samples.

3. Visibility Magnitude Only

   In this case so little light is available that all phase information will be lost, but visibility magnitudes can still be measured.

For even lower photon fluxes the fringe tracker itself will be used to measure visibility magnitudes. Refer to Appendix I on the visible fringe tracker for a more detailed discussion of the various modes of operation planned for the interferometer.

The imaging subsystem design employs single mode fibers to create a non-redundant linear output pseudo-array. The output of this array then passes through a dispersive element and an imaging lens assembly. Thus the fringes are formed in the image plane and are encoded spatially. A single-dimension output pseudo-array was chosen so that the second dimension of a two-dimensional detector could be used in a spectroscopic mode.

K.1.1. Design Approach

In reaching this design decision many conflicting requirements had to be balanced. Some of the design issues considered were:

- Should the fringe tracker use the same data as the imaging subsystem? As set out in Appendix I, it was decided that it should not. In this way the two systems can be developed independently, and a simpler upgrade path is available.

- Should one combine sub-groups of beams or try to combine all beams at once? In order to minimize the number of moving optical components and observation time, we have opted for combining all beams simultaneously.

- Should temporal or spatial fringe encoding be used? In temporal encoding, time dependent shifts in path length are applied to each beam. The fringes for each baseline will then be distributed in time. A detector with only a single pixel for each spectral channel is required, but it must be photon counting. Spatial encoding schemes normally use a non-redundant output array pattern for combination, thereby distributing the fringes across spatial frequency and requiring multi-pixel detectors. Because the CHARA Array contains so many optical channels (7), any temporal encoding scheme would be very complex. We have therefore opted for spatial encoding.

- Should the fringes be formed in the aperture or the image plane? The CHARA array forms fringes in the aperture plane for the fringe tracker and uses the image plane for the imaging subsystem.

In order to aid in the design effort, the layout of beam combiners used in other similar instruments were investigated, including those of the Cambridge Optical Aperture Synthesis Telescope (COAST) (Buscher 1988), the Navy Prototype Optical Interferometer (NPOI) (Mozurkewich 1993), the Calern High Angular Resolution Optical Network (CHARON) (Cruzalèbes et al. 1992) and the Sydney University Stellar Interferometer (SUSI) (Davis et al. 1993). It was also decided to try and take advantage of existing techniques for imaging, including those of the radio interferometry community. For example, the aperture masking technique is a proven method of imaging in the optical band (Bedding (1993), Tuthill et al. (1993), Buscher et al. (1990), Wilson et al. (1992)), and data reduction methods already exist for these systems. Furthermore, a great deal of software is available for image processing which can be used with little modification. To this end, the AIPS software package has been installed on the computer system at CHARA/GSU in order to gain experience with these sorts of software systems. The IDL package has been in use at CHARA/GSU for some years.

It has been pointed out by several authors (Buscher 1988, Prasad & Kulkarni 1989, Kulkarni et al. 1991) that there are very few theoretical distinctions between different beam combiner designs. The differences that do exist due to theory apply to the field of view criteria (refer to Appendix N) and the extreme low-light level cases. The distinguishing features of beam combiner designs are largely technological not theoretical. Of critical importance is the choice of detector system (refer to Appendix J), projected observation times, and ease of image analysis.

A final issue that must be kept in mind in the design process is to ensure that a viable and long term development/upgrade path exists. Multiple optical beam combination that achieves phase closure is neither a proven nor a fully understood technique. This is one of the reasons that the fringe tracking subsystem has been physically separated from the imaging subsystem. In this way, useful science can be extracted from the array long before an optical imaging subsystem is fully developed and operational.

K.2. REVIEW OF BEAM COMBINER DESIGNS

Before coming to a decision on the beam combiner optical layout, a review of existing designs was undertaken. Each beam combiner layout is described and discussed briefly below. A 'figure of merit' calculation was performed for each design. The final decision was based on this figure of merit along with some other implementation specific criteria.

K.2.1. Three Way Combination

This method is a simple extension of the fringe tracker design where a third split of the seven beams is combined with the set of pairs created for fringe tracking to form a three way combination of the beams. Figure K.1 shows a diagram of the optical layout for such a scheme. Note that this could also be implemented using single mode fibers and fiber couplers (Shaklan 1988) but would remain conceptually the same design. This scheme will provide seven sets of phase closure for each configuration along with visibility magnitude measurements of fifteen baselines. Five different configurations are required to sample all of the 15 phase closures and 21 baselines. Each change in configuration would require a re-alignment of the optical system. Since the imaging subsystem is coupled to the fringe tracking subsystem, it is not possible to select the baseline sample used for fringe tracking without affecting the baselines and phase closures measured by the imaging subsystem.

Another problem with this design is that it uses one set of the paired beams produced by the fringe tracking subsystem. This not only reduces the signal to noise in the fringe tracker but makes it difficult, if not impossible, to use the fringe tracker for visibility magnitude measurements as set out in Appendix I. As three beams are combined in each imaging channel, a temporal encoding scheme will be necessary in order to de-couple the separate baselines. Either this encoding occurs after the fringe tracker or it will have to be incorporated into the fringe tracking scheme. Furthermore, since single-pixel detectors would be used, most probably avalanche photo-diodes (Nightingale 1991), the bandwidth used in the imaging subsystem will have to be restricted to retain a large enough coherence length (refer to Appendix N).

This design not only restricts the number of baselines and phase closures that can be measured at any time but also reduces the usable bandwidth of the Array. It is strongly coupled to the fringe tracking system thereby clouding the design issue of the two systems and reducing the functionality of the fringe tracer. Finally, a temporal fringe encoding scheme is required which, while not in itself a major drawback, would interfere with the operation of the fringe tracking subsystem.

K.2.2. All Beam Combination

This design, shown in Figure K.2, is based on the COAST beam combining system (Buscher 1988). Note that the optical layout is symmetric, and the layout is drawn up for eight beams instead of seven. In this design, all possible combinations of beams are represented in each output channel and therefore only one configuration is required to measure all baselines and phase closures. Path length is preserved in this optical system although not all of the final output beams have undergone the same number of reflections and transmissions which may cause differential polarization effects.

Since each output beam contains information from all telescopes, a temporal fringe encoding scheme is required. Buscher (1988) shows how this would function for a four-beam version

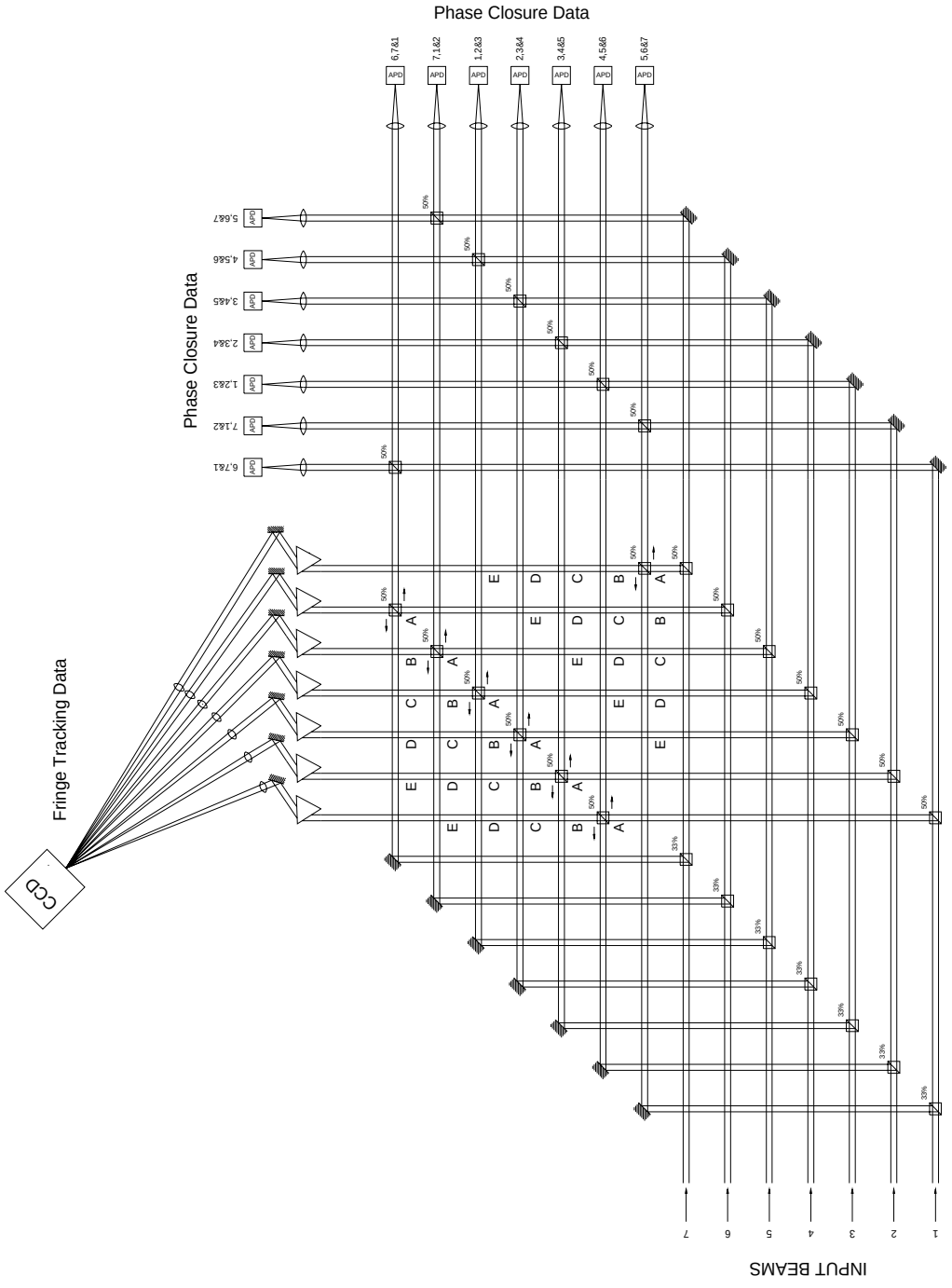

FIGURE K.1. Optical layout for a fringe tracker/three-way beam combining scheme.

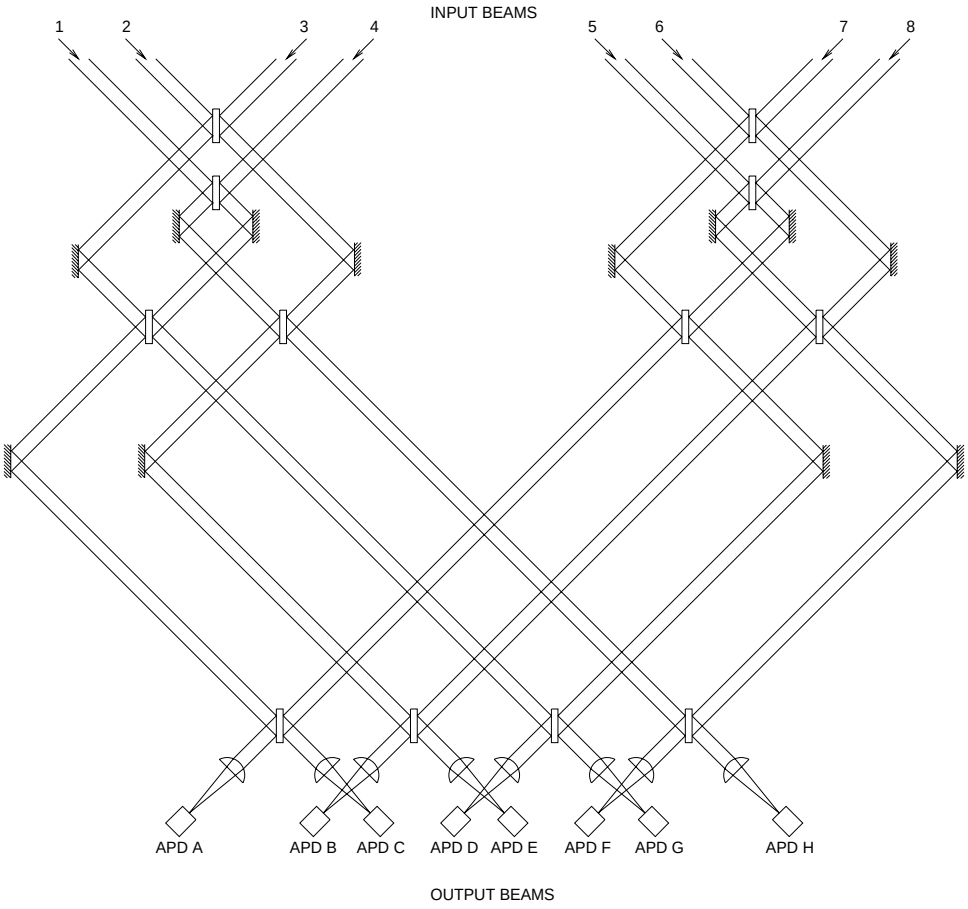

FIGURE K.2. Optical layout for an all-beam combination scheme based on the COAST array scheme. Each of the eight outputs contains the data for all baselines. Note that this scheme requires that the number of beams is a power of 2.

of this system. Unfortunately, to expand this encoding algorithm to seven or eight beams makes the encoding and consequent decoding routines much more complicated. In fact, it is not clear that such an encoding system can be made to work at all.

As with the three-beam system described above, single-pixel detectors are used implying that the bandwidth must also be restricted. Another drawback of this layout is the difficulty and extra reflections involved in getting the eight input beams into the appropriate geometry for entering the beam combiner. The seven or eight beams will approach this beam combiner in a parallel configuration (refer to Appendix H). Some extra mirrors would be required to transfer this set of parallel beams into the input geometry shown in Figure K.2 that neither affect polarization nor introduce optical path length differences. This adds unnecessary complexity to the beam combining optics and many more reflections. A fiber implementation of this design would not suffer from these geometrical and polarization problems, but the fringe encoding problems would still have to be overcome, and the throughput would be reduced significantly.

K.2.3. One-Dimensional Non-Redundant Pseudo Array

Instead of encoding the fringes in time, thereby introducing a complex series of path length changes into the beams, one could use a spatial encoding scheme. If the evenly spaced beams are rearranged such that the spacing between them is non-redundant, that is no two pairs of beams have the same spacing, each baseline will form a fringe pattern in the image plane with a unique spatial frequency. Thus the fringes corresponding to each baseline can be separated without the need to introduce path length modulation. If the spatial encoding is done in one dimension, the second dimension can then be used for spectroscopy. An effectively large bandwidth is then achieved by using many small bandwidths. In this way the bandwidth of this beam combining system is not restricted as are those that use temporal fringe encoding.

An example of an optical layout for getting four, originally equally spaced, beams into a non-redundant pattern is given in Figure K.3. The box labeled 'Beam Combiner and Spectrograph' would be the same as that shown in Figure K.7 in Section K.2.6 and consists of a dispersive element and imaging optics.

The optics used to change the evenly spaced beams into a non-redundant pattern must introduce neither differential paths nor different numbers of reflections into the beams. The layout shown in Figure K.3 achieves this and is based on a layout presented by Roddier (1987). Each beam undergoes the same number of reflections, some of which, like that in beam 4, are added simply to maintain symmetry. The number of reflections required goes up quickly as more beams are added, making the design and alignment of such a scheme complex.

A final focusing element is also required for such a scheme to work. With large numbers of beams this optical component can get very large. For example, the smallest non-redundant linear spacing possible for seven beams is 2-1-7-6-5-4, which has a maximum spacing of 25. The minimum spacing must be at least twice the size of the beam diameter, otherwise it will be impossible to adequately separate the spatial frequencies. So for the beam diameter of 25 mm planned for the CHARA Array, the size of the focusing element would be 125 cm. This is not only somewhat unwieldy but would be costly to produce. A way around this problem is to only combine a subset of the beams. Unfortunately, this means you need multiple observations to collect all baseline and phase closure data and implies the use of moving optical components.

A number of authors, for example Traub (1986), have pointed out that unless the output pseudo array has the same geometry as the input array, the field of view can be severely restricted. While using a non-redundant output array will restrict the field of view the calculations in Appendix Q show that it should still be sufficient to cover the intended target objects of the array.

K.2.4. Seven Beam Non-redundant Pseudo Array

In order to avoid using a single large focusing element to create the fringes in the image plane it may be possible to use a set of prisms to combine the beams as shown in Figure K.4. This is similar to the Fresnel lens approach and would require expensive custom made optics. The advantage of this layout is that all seven beams can be combined at once and the observing time for any given object will be reduced. Unfortunately, the design and manufacture of the prisms would not be straight forward, especially if a wide bandwidth was desired. It is also not clear how one would get the seven beams into the non-redundant pattern in the first place. Furthermore, with the non-symmetric arrangement of the beams

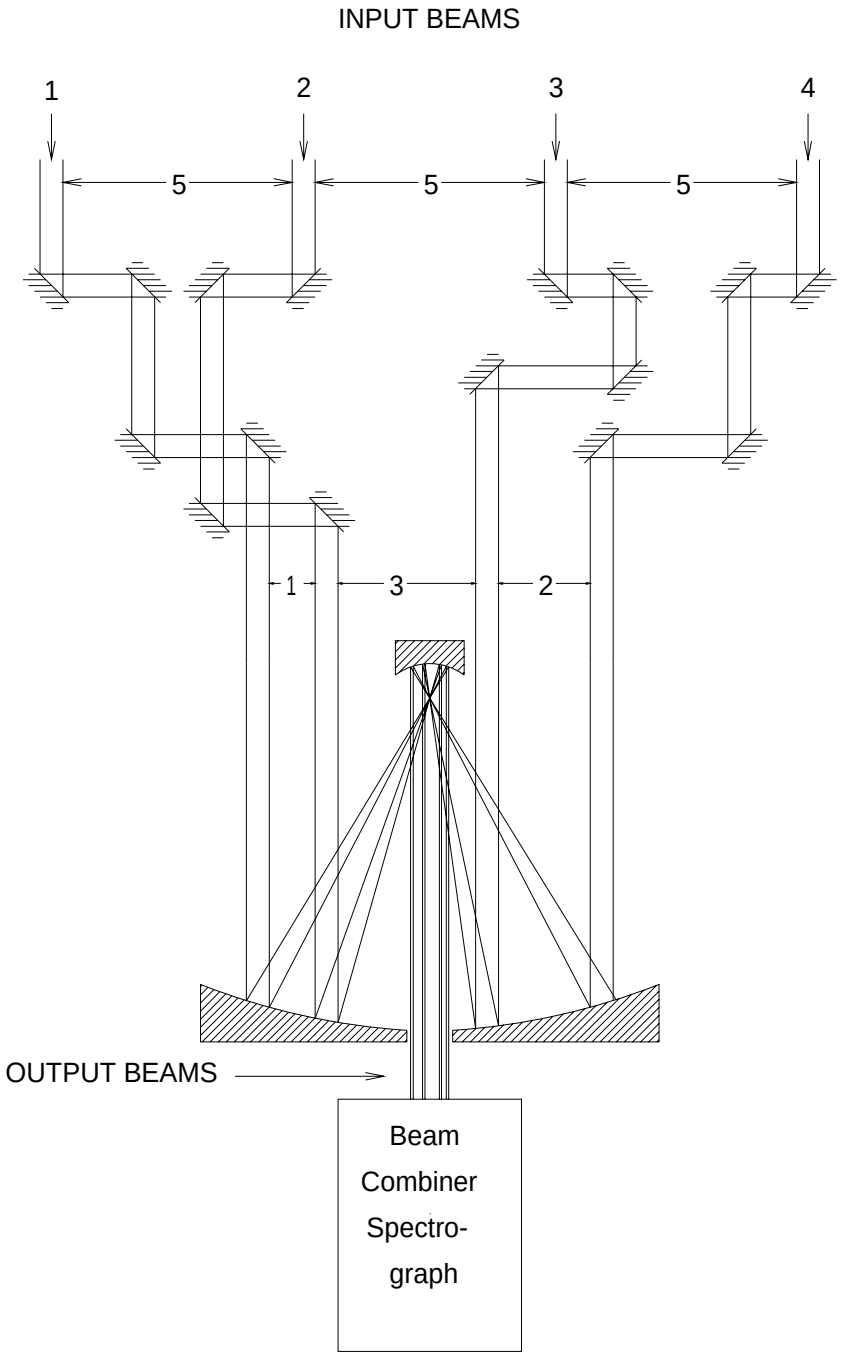

FIGURE K.3. A system for getting four evenly-spaced beams into a non-redundant pattern without introducing differential path lengths or different numbers of reflections.

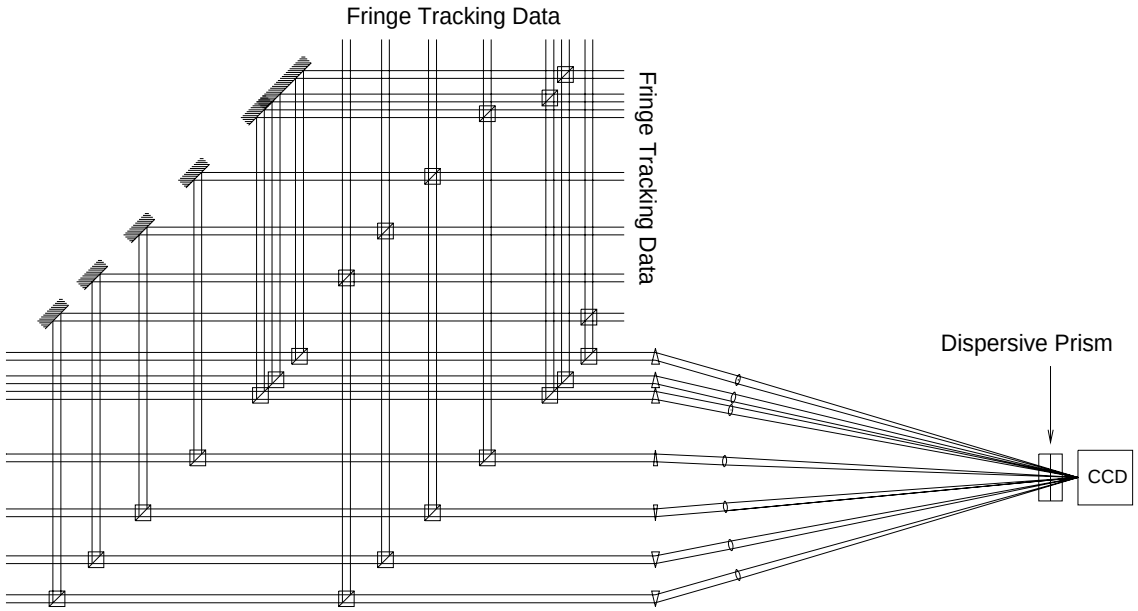

FIGURE K.4. Using prisms to combine seven non-redundantly spaced beams. Each prism represents a small part of a large lens in a similar manner to a Fresnel Lens.

the line of equal phase is a curve so that the optics as shown in Figure K.4 would not actually have both the fringe tracking section and the imaging section simultaneously in phase. A more complex optical system than that shown in Figure K.4 would be required to correct for these effects.

K.2.5. Two-Dimensional Non-Redundant Pseudo Array

One way of avoiding the problems of a large focusing element and the need for moving parts would be to use a two-dimensional non-redundant output array. There are many such patterns for seven beams. One example of a seven-beam non-redundant pattern is given in Figure K.5, while a schematic of an optical

configuration to implement it is shown in Figure K.6.

The size of the focusing element required in this scheme is only twelve times the beam width, which in the case of the CHARA Array would be 30 cm. This makes building this system much more practical than a one-dimensional array containing all seven beams. All baselines and all phase closures are simultaneously available with this configuration, and all beams undergo the same number of reflections.

There are, however, a number of drawbacks in this design. Since the beams are co-planar when they approach the beam combiner, both periscopes and mirrors are required to re-arrange the beams into a two-dimensional pattern. Some of the mirrors will be quite high above the optical table which could introduce stability problems. Furthermore, it is not clear how to arrange these periscopes and mirrors without introducing differential paths making the extra cat's eyes necessary. Because we have used both dimensions of the detector for fringe encoding, it is no longer possible to use one dimension for spectral dispersion. Thus a narrow-band filter has been added to the layout reducing the optical bandwidth of the device. The cost of the optics for this scheme would also be prohibitive.

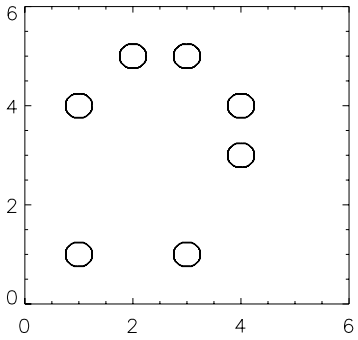

FIGURE K.5. Beam positions for a two-dimensional non-redundant pattern.

K.2.6. Single-Mode Optical Fiber Beam Combiner

The major drawback of using the seven beam one dimensional non-redundant array described in Section K.2.3 is the large size of focusing optics. A way around this problem is to use single-mode fibers to reduce the physical size of the output array. An optical layout to achieve this is given in Figure K.7.

Single-mode fibers are required since in multimode fibers the different modes have different propagation times. No fringes would be observed since different modes would interfere with each other and coherence would be lost. Using single mode fibers for interferometry has been suggested by others, for example Shaklan (1988), and has many advantages. For example, the fibers preserve phase and will reduce the size of the non-redundant array such that standard 'off the shelf' optics can be used. Thus all the advantages of the one-dimensional, non-redundant output array described in Section K.2.3 apply without the problems of custom built large optical components: large bandwidths can be used; all baselines and phase closure information is present; and, standard optics can be employed. While potential polarization problems can develop when using single mode fibers, techniques exist for overcoming them.

Once the fibers are brought together into a non-redundant pattern a series of collimating lenses will be required. This is the only custom built optics required for this design. The next optical element will be a prism to disperse the light across the vertical axis. This prism can be adjusted to enable the choice of bandpass used. Once dispersed, the beams enter the imaging optics shown at the bottom of Figure K.7. This optical configuration includes two cylindrical elements resulting in a long focal length in the horizontal plane and a short focal length in the vertical plane. In this way a large Airy spot, across which the fringes will appear, is created across the horizontal axis while the vertical size of the disk will be very small. This flattened spot is dispersed in wavelength along the vertical axis of the detector. The system can be looked upon as two separate optical assemblies, an interferometer in the horizontal plane and a spectrograph in the vertical plane.

The Airy disk formed on the detector is an image of the end of the fibers, not of the target object. The fibers form the equivalent of the slit in a standard spectrograph, and the system will therefore be largely insensitive to image wander. Furthermore, while photon flux will be lost due to coupling inefficiency, any light that does reach the combining optics will be spatially filtered to a high degree, a lot of the light lost while coupling to the fibers would

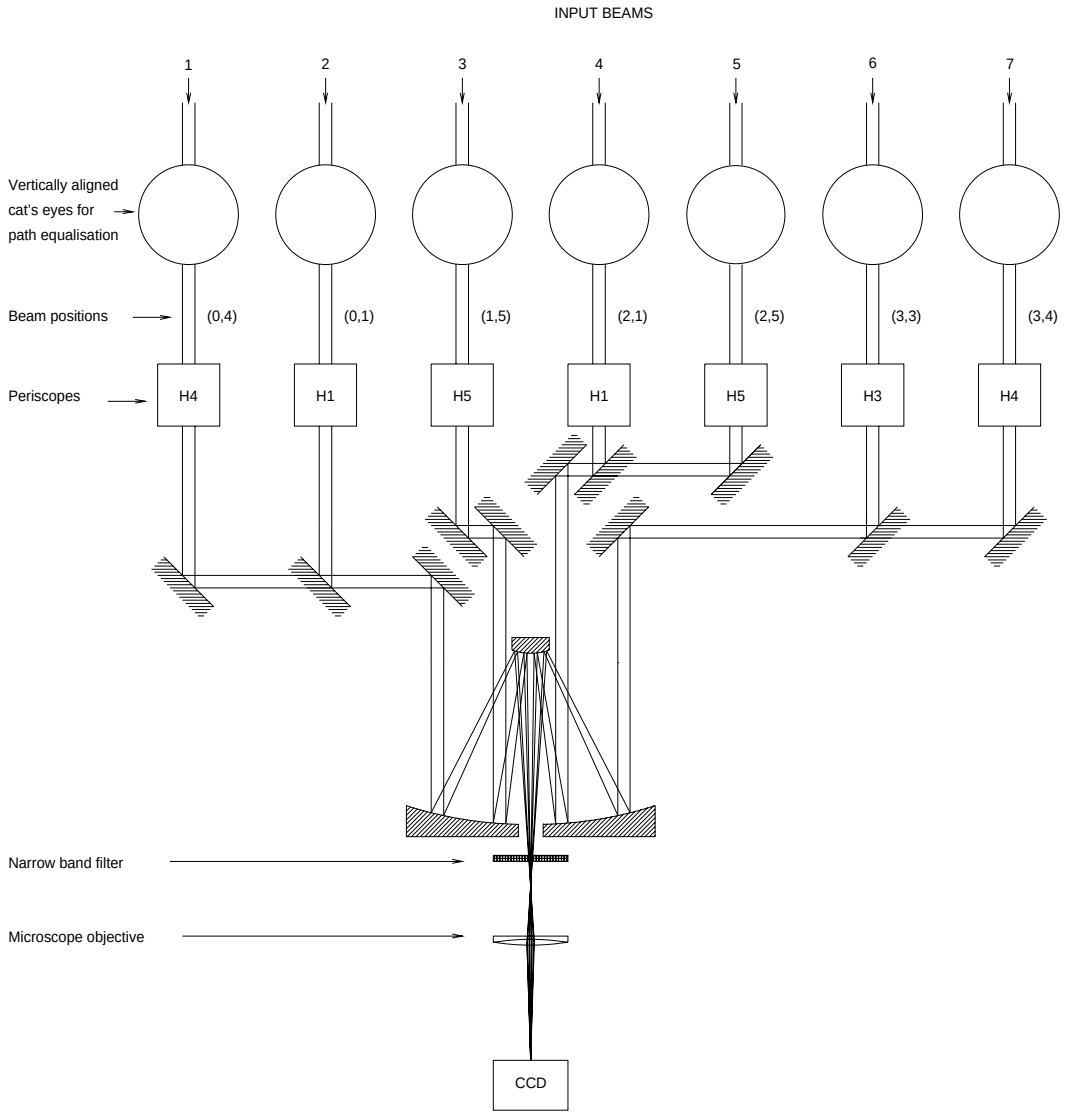

FIGURE K.6. Optical layout for a beam combiner employing a two-dimensional non-redundant output array. The positions for each beam in the two-dimensional plane are written above each line. The cat's eyes are used to equalize the beam paths, and the periscopes bring each beam to the correct height. While it appears that some beams pass through mirrors, these mirrors and beams are in different vertical positions.

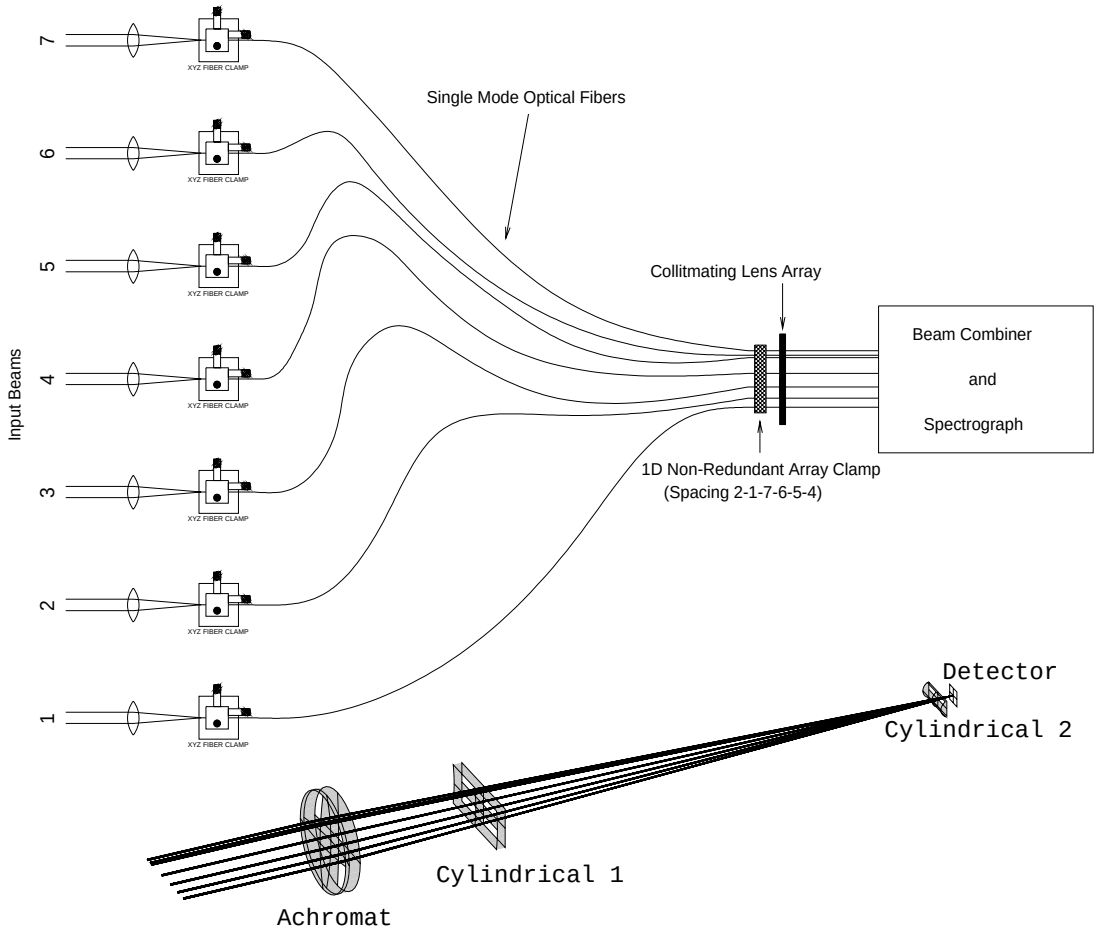

FIGURE K.7. **Above:** A beam combiner using single mode optical fibers. **Below:** Optics used to form fringes given a non-redundant input array. A prism will precede these optics so that the image will be dispersed vertically in wavelength, while the fringes are formed in the horizontal axis. The two cylindrical elements are inserted so that the focal length of the horizontal axis is much greater than the vertical axis.

not have formed useful fringes anyway. This is equivalent to using a spatial filtering system which, at least for a simple pinhole spatial filter, has been shown by Prasad & Loos (1993) to improve interferometer performance.

Another advantage of using optical fibers is that the imaging subsystem becomes completely independent of the fringe tracker; it need not even be on the same optical table. No matter which fringe tracking scheme is employed or what the final relative phasing of the beams is, the fiber couplers can be placed at the appropriate positions to ensure the highest contrast fringes.

The major concern with this approach is coupling the light into and out of the fibers. At the input side, a single achromatic lens is used to focus the beam onto a standard fiber mount. It will be imperative to ensure that the fiber tips are optically superimposed on the tip/tilt detector centers. Any aberration of the beam phase will also affect coupling efficiency (Wagner & Tomlinson 1982) although, as pointed out above, any phase curvatures that reach the combining optics would only result in reducing fringe visibility.

K.2.7. Figure of Merit Calculations

While it is difficult to factor in all considerations, especially those of alignment difficulty and cost of custom optics, a figure of merit equation can aid in making the final design choice. The figure of merit equation used to help compare the imaging schemes outlined above is

$$\mathrm{FOM} = \frac{0.95^{(R+T)} \times B \times \mathrm{DQE}}{N} \tag{K.1}$$

where R is the number of reflections, T is the number of transmissions, B is the optical bandwidth in nanometers, DQE is the detector quantum efficiency and N is the number of different configurations required to measure all possible baselines and phase closures. In this equation, it is assumed that high reflectivity mirrors and high quality transmission elements will be used each achieving 95% efficiency. Because these figures will appear in all calculations, the exact value is not extremely significant. This equation does not take into account the ease or difficulty of building each system or the cost of purchasing the components. Table K.1 shows the resulting figures of merit for each of the systems described above.

Some of the numbers appearing in this table may need some clarification. When a system uses temporal encoding or requires a restricted bandpass in order to maintain coherence, the optical bandwidth has been set to 10 nm. In all other cases the bandwidth has been set to 100 nm with the exception of the seven beam one-dimensional array employing prisms. The bandwidth of this device has been set to 50 nm due to the difficulty in building achromatic prisms. The quantum efficiency of a photon counting array (PCA) detector has been set to 15% while that of an avalanche photo diode at 40%. It is difficult to predict what sort of coupling efficiency is to be expected with the single-mode fibers. In theory this can be over 70% while in practice experiments at NOAO coupling single mode fibers directly to telescopes have only achieved 10%. With tip/tilt correction, this should be improved, and so the coupling efficiency has been set to 25%. This is probably a conservative estimate.

In order to try and factor in the more subjective issues, a second set of merit numbers were assigned to each design. Table K.2 shows the resulting values with each system being given a score out of 5 in each category. The categories included are described in the caption

TABLE K.1. Figure of merit values, based on Equation K.1.

Beam Combination Scheme	N	R	T	Detector QE	B nm	Comments	FOM
Three way Combination	5	2	3	APD 40%	10	Many Optical Components.	0.6
All Beam Combination	1	4	4	APD 40%	10	Non-symmetric reflections may affect polarization. Non-parallel input beams.	2.7
4-Beam Non-Redundant 1D Array	7	6	4	PCA 15%	100	Large combining optics.	1.3
7-Beam Non-Redundant 1D Array	1	5	3	PCA 15%	50	Interferes with fringe tracker. Difficult prism design. Extra optics required for input configuration. Large table required.	5.0
7-Beam Non-Redundant 2D Array	1	8	3	PCA 15%	10	Large combining optics. Extra cat's eyes required to equalize beam paths.	0.9
Optical Fiber Fed Non-Redundant 1D Array	1	0	6	PCA 15% Fiber 25%	100	Spatial Filter. Polarization problems and losses due to fibers. Compact and stable.	2.8

to Table K.2. The next column in Table K.2 contains the final figure of merit value as a fraction of 1.0. The final numbers in each row are the figure of merits from Table K.1 and an overall score for the design.

The layout with the highest final score is the fiber-fed non-redundant array design, although the seven-beam non-redundant array employing prisms is a very close second. If a higher fiber coupling efficiency was assumed or a different bandwidth, the comparison will change significantly. It is because of implementation difficulties that the prism design has been eliminated. The prisms used would have to be 'achromatic' in the sense that they would need to refract all wavelengths in the pass band equally. They would not be simple flat edged prisms but would have curved surfaces. Thus this system scored zero for component availability. Apart from the problems associated with the prisms, this design assumes that the beams are already in a non-redundant pattern (thus the five reflections listed for this scheme in Table K.1). As pointed out in Section K.2.3 the width of a seven-beam non-redundant array would be 125 cm, making the optical surface that contains the fringe tracking and imaging systems very large and consequently expensive. The 'focal length' of the prism set would need to be large to avoid aberrations, making the required table size still larger. Finally, having the beams in a non-redundant pattern interferes with the functionality of the fringe tracking subsystem. All in all, because of these implementation problems this design must, for the time being, be eliminated. The beam combining scheme chosen is therefore the one employing single-mode optical fibers.

TABLE K.2. 'Subjective' figure of merit values. The first seven columns are for the categories; A - Cost, B - Availability of optics, C - Difficulty of setup and alignment, D - Moving optical components, E - Coupling with fringe tracking subsystem, F - Polarization effects and G - Physical layout size. The next three colums are the resulting score out of 1 based on these ratings, the previous figure of merit value from Table K.1 followed by a final score for the design.

Beam Combination Scheme	A	B	C	D	E	F	G	SubTotal	FOM	SCORE
Three way Combination	5	5	5	1	1	5	3	0.69	0.6	0.41
All Beam Combination	4	4	4	4	5	2	4	0.77	2.7	2.08
4-Beam Non-Redundant 1D Array	3	4	3	1	5	5	3	0.69	1.3	0.90
7-Beam Non-Redundant 1D Array	1	0	2	5	2	5	1	0.46	5.0	2.30
7-Beam non-Redundant 2D Array	2	3	3	5	4	5	2	0.66	0.9	0.60
Optical Fiber-Fed Non-Redundant 1D Array	4	4	4	5	5	5	5	0.91	2.8	2.55

K.3. BEAM COMBINING SUBSYSTEM OPTICAL LAYOUT

Figure K.8 shows a diagram of the entire beam combining system including the fringe tracking scheme discussed in Appendix I, some of the alignment optics discussed in Appendix M, the tip/tilt quadrant detectors, and the imaging subsystem. A hardware tree for the imaging system is given in figure Figure K.9. Note that the tip/tilt detectors are included in the fringe tracker hardware tree in Appendix I. Each assembly of the beam combining system will be described separately.

K.3.1. Beam Input Assembly

The infra-red and visible light components are separated in the beam sampling subsystem (refer to Appendix H). After this, the seven visible-light beams enter the beam combining area. The first components in the optical chain are seven autocollimation mirrors and are part of the alignment subsystem. Note that these mirrors are along a diagonal line and parallel to the fiber coupling assemblies. As explained in Appendix I, the line of equal phase created by the fringe tracker is along this diagonal. After the alignment optics the beams are split into the two polarizations, one dedicated to fringe tracking and the other shared between wavefront tilt detection and imaging. Following the polarizing beam splitters are a set of shutters so that sub-sets or individual beams can be selected within the fringe tracker

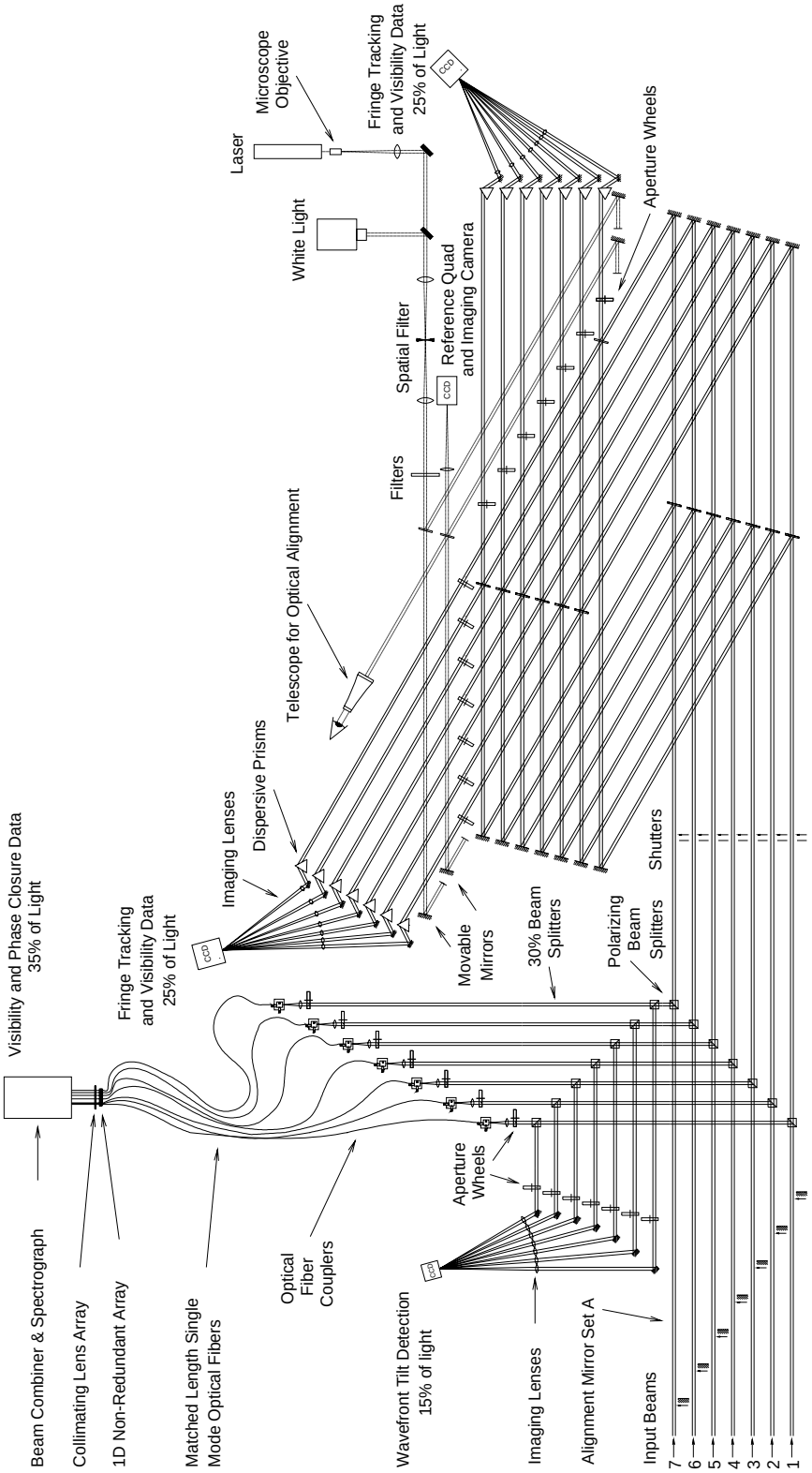

FIGURE K.8. Layout of the beam combining optics.

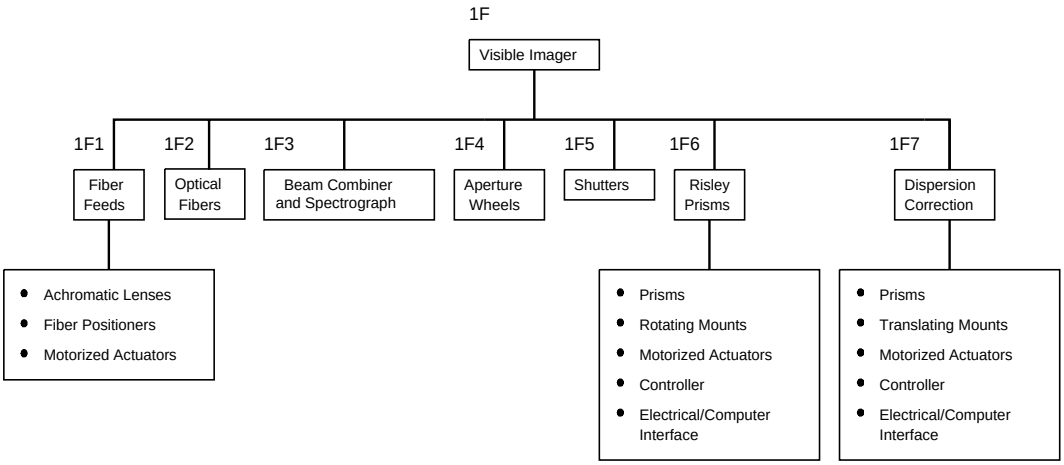

FIGURE K.9. Hardware tree for the visible light imaging subsystem.

without affecting either the tip/tilt detection or imaging.

K.3.2. Fringe Tracking Subsystem

This subsystem is described in more detail in Appendix I and appears in this diagram only for completeness. The only differences between the fringe tracking layout shown in Figure I.1 of Appendix I are the addition of some alignment optics, aperture stops and a skewing of the optical geometry in order to avoid 90 degree reflections and reduce polarization problems. The aperture wheels allow the observer to select an aperture size appropriate for the prevailing seeing conditions and object brightness.

K.3.3. Tip/Tilt Detection

The tip/tilt detectors form part of the tip/tilt or 'wobbler' servo responsible for keeping the image of each optical channel stable and optically superimposed. A set of aperture wheels are included so that an appropriate aperture size can be selected. This aperture size is not necessarily the same as that used elsewhere and will normally represent the entire telescope aperture. The tilt measurement technique to be used is quadrant detection (refer to Appendix O) with all seven quadrants implemented on a single CCD chip. Only 15% of the available light is allotted to tip/tilt measurement, but, as the entire aperture would normally be used, this system will function at lower light levels than any of the other opto-electrical servos. The mirrors reflecting the sampled beams into the quadrant detector cells will have alt/az adjustment capability in order to aid in the superposition of all the beams. By moving these mirrors, the apparent position of each beam can be changed on the quadrant detector. This will force the tip/tilt servo to move the beam such that it is re-centered, and in this way proper beam alignment can be achieved.

K.3.4. Alignment Optics

The optical alignment scheme is more fully described in Section M. In summary two light sources, a laser and a white light, share a spatial filter which defines the reference optical

axis for the entire interferometer. These beams can be fed into any of the fringe tracker beam splitters, autocollimated at a selected position in the optical chain and inspected, either by eye, with a CCD imager or a quadrant detector. The reference quadrant detector will be optically superimposed on the pin hole and will aid in remote re-alignment of the input beams.

K.3.5. Imaging Subsystem

After 50% of the light has been split off for fringe tracking and a further 15% for tip/tilt detection, the remaining 35% reaches the imaging subsystem. Another set of aperture wheels are placed before the optical fiber coupling assemblies so that a different aperture size can be used for imaging than those used for fringe tracking and tilt detection. The fiber coupling assemblies lie along the diagonal of equal phase, and the fibers themselves will be matched in length in order to preserve coherence. The coupling assemblies themselves will be mounted on movable platforms in order to facilitate the adjustment of the path lengths within the imaging subsystem. The fibers themselves will also include fiber to fiber couplers. In this way the arrangement of the seven beams in the non-redundant linear array block can be changed, and the fiber lengths can be adjusted by replacement of one end of the fiber. Furthermore having break points in the fiber lengths will facilitate experiments into other types of fiber combination schemes without disturbing the rest of the optical alignment. The rest of the imaging optics are as described in Section K.2.6. The alignment and efficiency of the coupling assemblies will have the greatest effect on the imaging subsystems optical efficiency. A computer simulation is being developed and an experimental laboratory established at GSU in order to investigate coupling of light into single mode fibers and alignment techniques of a fiber-based beam combiner.

K.4. DATA REDUCTION TECHNIQUES

The data reduction techniques planned for the imaging subsystem are based on the methods used in aperture masking experiments. The thesis by Buscher contains an excellent review of these procedures. Basically, since the fringes are encoded by spatial frequency, a Fourier transform of each spectral channel will contain peaks corresponding to each baseline. An example of the type of fringes obtained within the imager is given in Figure K.10.

In order to gain experience in these data reduction techniques as well as make some worthwhile scientific measurements, a simple four-hole non-redundant mask is in operation on the 16-inch telescope at Hard Labour Creek Observatory belonging to GSU. Phase closure has been achieved with this system, and an example of the results obtained is given in Figure K.11.

If the geometry of the imaging subsystem is known precisely, the position of the peak corresponding to each baseline in the Fourier transform will be known in advance. Since in practice this will not be the case, a summation of the power spectrum of many frames will reveal the peak positions. The magnitude and phase of each peak is directly calculated by the Fourier transform. Thus closure phases and visibility magnitudes can be found. If individual frames have too little signal to noise, the peak heights and phase closures can be averaged over many frames.

The detector used in these experiments runs at video rates, and so the smallest sample time available is 30 ms which is, unfortunately, much longer than the time constant for

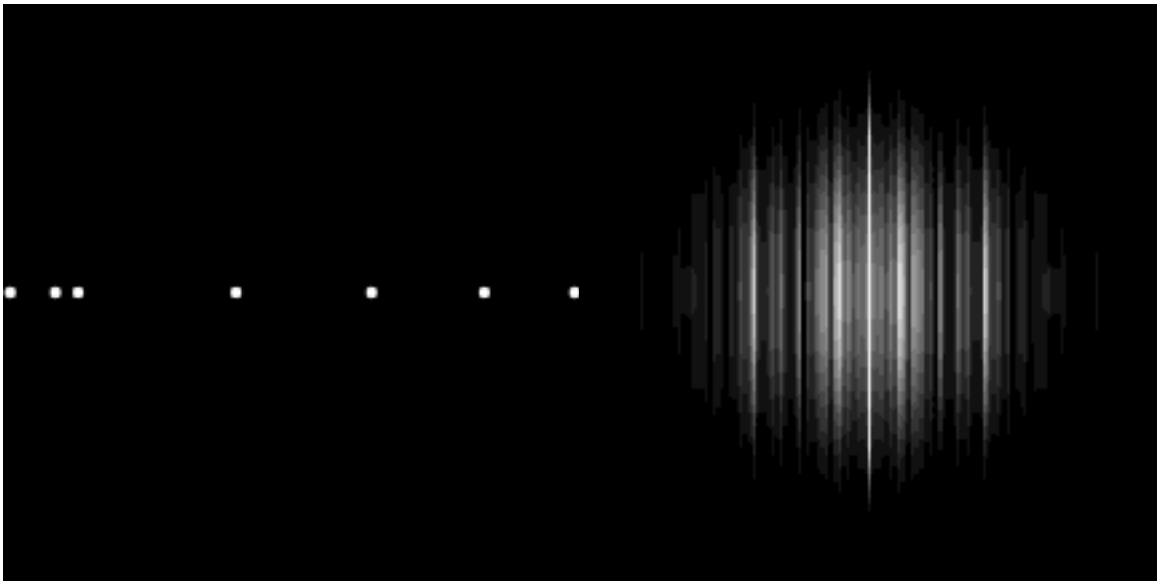

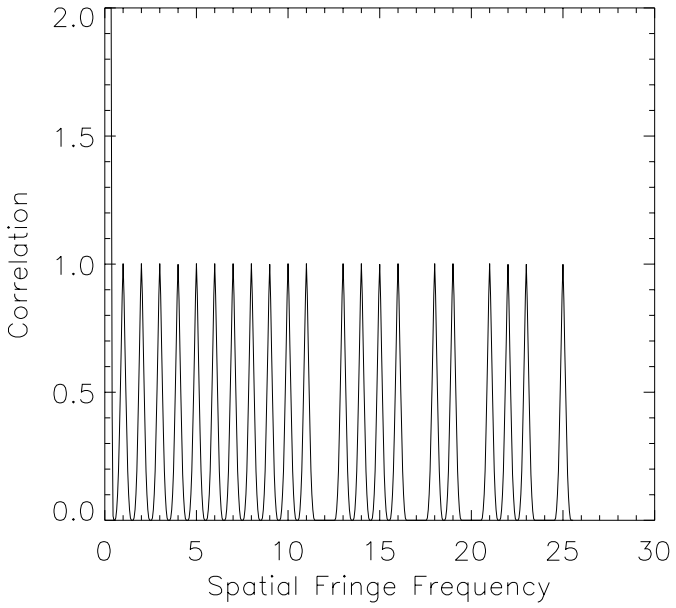

FIGURE K.10. Example of the kind of fringe pattern measured by the imaging subsystem. The seven-beam non-redundant pattern is illustrated in the top left while the resulting fringe pattern is shown in the top right. A pattern like this, only squashed down in the vertical axis, will be present in each spectral channel of the detector assembly. The plot below is the power spectrum of the fringe pattern. A peak is present for each pair of apertures. Note that while all twenty one baselines are represented, due to the output array spacing, some spatial frequencies are missing.

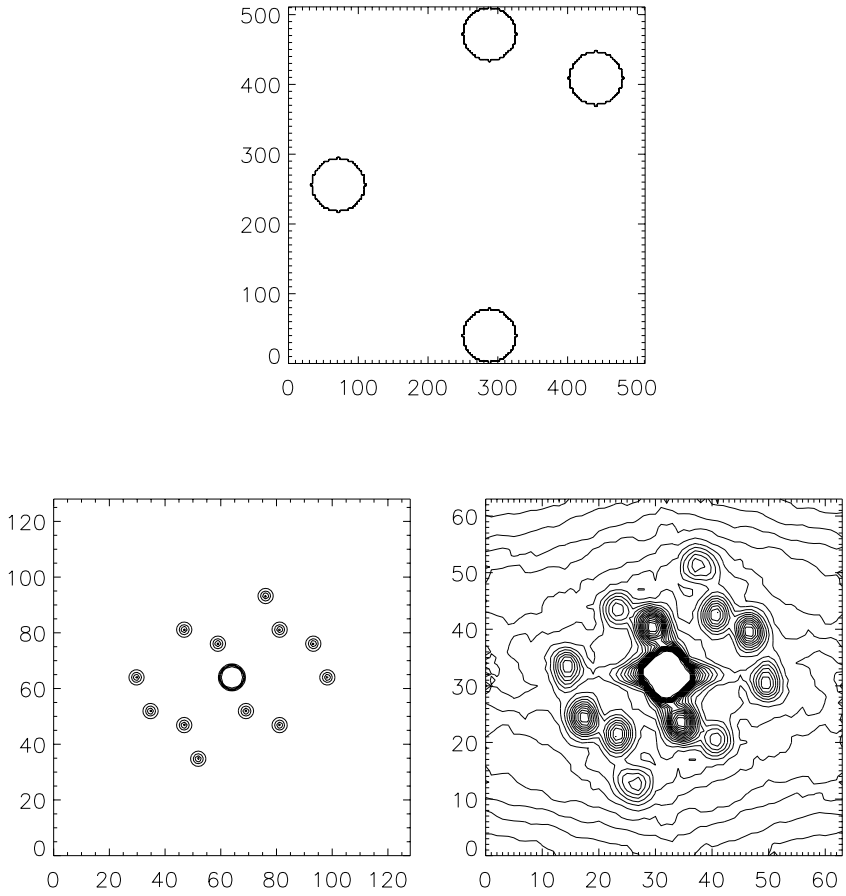

FIGURE K.11. Some actual aperture masking data. The top diagram shows the layout of the non-redundant mask used. The two plots below show the theoretical power spectrum of the resulting fringe pattern on the left and the power spectrum of actual data collected at HLCO.

atmospheric turbulence. Nevertheless fringes are easily observed and the power spectrum shown in Figure K.11 clearly shows peaks corresponding to all six baselines. Note that these power spectra are only used to locate the peaks. Once their positions are known, the magnitude and phase closures of each frame are averaged to produce a measurement.

Numerical modeling of aperture masks have also been studied at GSU in order to get a feel for low photon flux behavior of these systems. It was found that for a four-hole mask, such as the one described above, at least three photons per aperture per frame are required in order to measure phase closure. If only visibility magnitude is measured, one can go down to two photons per frame per aperture. These models did not, however, include any readout noise of the detector used. More photons would need to be collected per frame to overcome this noise. Modeling continues in order to study these problems.

If the fringe tracking subsystem is able to hold the fringes stable and the target object is

bright, only one frame will be necessary to measure phase closures and visibility magnitudes. At lower photon fluxes, many shorter frames will need to be logged and processed in a similar manner to the aperture masking data discussed above.

K.5. REFERENCES

Bedding, T. R.1993,"The orbit of the binary star Delta Scorpii",*AJ*, **106**, 768

Buscher, D. F., 1988, *Getting the most out of the C.O.A.S.T.*, (Cambridge University, Cambridge)

Buscher, D. F., Haniff, C. A., Baldwin, J. E., & Warner, P. J., 1990, "Detection of a Bright Feature on the Surface of Betelgeuse,", *MNRAS*(Short Communication), **245**, 7p

Cruzalèbes, P., G. Schumacher, G., & Starck, J., 1992, "Model-independent Mapping by Optical Aperture Synthesis: Basic Principles and Computer Simulation", *JOSA-A*, **9**, 708

Davis, J., 1993, "The Sydney University Stellar Interferometer (SUSI) ", in *Proc: Iau Symp 158 on Very High Angular Resolution Astronomy,* Ed: Tango, W.J. and Robertson, G., in press

Kulkarni, S. R., Prasad, S., & Nakajima, T., 1991, "Noise in Optical Synthesis Images. II. Sensitivity of an ${}^nC_2$ Interferometer with Bispectrum Imaging", *JOSA-A*, **8**, 499

Mozurkewich, D., 1993, "Design and Construction of a Beam Combiner and Related Hardware " in *Proc: IAU Sym 158 on Very High Angular Resolution in Astronomy,* Ed: Tango, W.J. and Robertson, G., in press

Nightingale, N. S., 1991, "A New Silicon Avalanche Photodiode Photon Counting Detector for Astronomy," Experimental Astronomy, **1(6)**, 407

Prasad, S. & Kulkarni, S. R., 1989, "Noise in Optical Synthesis Images. I. Ideal Michelson Interferometer," JOSA-A, **6**, 1702

Prasad, S. & Loos, G., 1993, "Spatial Filtering of Atmospheric Decorrelation from Wavefronts for Interferometry," Optics Communications, **99**, 380

Roddier, F., 1987, "Redundant versus Nonredundant Beam Recombination in an Aperture Synthesis with Coherent Optical Arrays," JOSA-A, **4**, 1396

Shaklan, S., 1988, "A Long-Baseline Interferometer Employing Single-Mode Fiber Optics " in *Proceedings: PASP V.3: Fiber Optics in Astronomy,* XVII, 262

Thompson, A. R., Moran, J. M., & Swenson, G. W., 1986, *Interferometry and Synthesis in Radio Astronomy* (John Wiley and Sons, New York)

Traub, W. A., 1986, "Combining Beams from Separated Telescopes," Applied Optics, **25**, 528

Tuthill, P. G., Haniff, C. A., & Baldwin, J. E., 1993, "An Interferometric Survey of Mira Variables and M Supergiants " in *Proc: IAU Symp 158 on Very High Angular Resolution Astronomy,* Ed: Tango, W.J. and Robertson, G., in press

Wagner, R. E. & Tomlinson, W. J., 1982, "Coupling Efficiency of Optics in Single Mode Fiber Components," Applied Optics, **21**, 2671

Wilson, R. H., Baldwin, J. E., Buscher, D. F., & Warner, P. J., 1992, "High-Resolution Imaging of Betelgeuse and Mira,", *MNRAS*, **257,** 369